Eidgenössische Technische Hochschule Zürich

Ecole polytechnique fédérale de Zurich
Politecnico federale di Zurigo
Swiss Federal Institute of Technology Zurich

Enhanced approximate cloaking by SH and FSH lining

J. Li, H. Liu* and H. Sun†

Research Report No. 2011-65
October 2011

Seminar für Angewandte Mathematik
Eidgenössische Technische Hochschule
CH-8092 Zürich
Switzerland

*Department of Mathematics and Statistics, University of North Carolina, Charlotte, NC 28263, USA

†Institute of Mathematics, Academy of Mathematics and Systems Science, Chinese Academy of Sciences, Beijing 100190, P. R. China

Enhanced Approximate Cloaking by SH and FSH Lining

Jingzhi Li* Hongyu Liu† Hongpeng Sun‡

Abstract

We consider approximate cloaking from a regularization viewpoint introduced in [13] for EIT and further investigated in [12, 17] for the Helmholtz equation. The cloaking schemes in [12] and [17] are shown to be (optimally) within $|\ln \rho|^{-1}$ in 2D and ρ in 3D of perfect cloaking, where ρ denotes the regularization parameter. In this paper, we show that by employing a sound-hard layer right outside the cloaked region, one could (optimally) achieve ρ^N in $\mathbb{R}^N,\ N \geq 2$, which significantly enhances the near-cloak. We then develop a cloaking scheme by making use of a lossy layer with well-chosen parameters. The lossy-layer cloaking scheme is shown to possess the same cloaking performance as the one with a sound-hard layer. Moreover, it is shown that the lossy layer could be taken as a finite realization of the sound-hard layer. Numerical experiments are also presented to assess the cloaking performances of all the cloaking schemes for comparisons.

1 Introduction

A region is said to be *cloaked* if its contents together with the cloak are invisible to certain measurements. From a practical viewpoint, these measurements are made in the exterior of the cloak. Blueprints for making objects invisible to electromagnetic waves were proposed by Pendry *et al.* [24] and Leonhardt [16] in 2006. In the case of electrostatics, the same idea was discussed by Greenleaf *et al.* [10] in 2003. The key ingredient is that optical parameters have transformation properties and could be *pushed-forward* to form new material parameters. The obtained materials/media are called *transformation media*. We refer to [4, 7, 8, 23, 26, 28] for state-of-the-art surveys on the rapidly growing literature and many striking applications of the so-called 'transformation optics'.

In this work, we shall be mainly concerned with the acoustic cloaking via 'transformation acoustics'. The transformation media proposed in [10, 24] are rather singular. This poses much challenge to both theoretical analysis and practical fabrication.

*SAM, D-MATH, ETH Zürich, CH–8902, Switzerland (jingzhi.li@sam.math.ethz.ch)

†Department of Mathematics and Statistics, University of North Carolina, Charlotte, NC 28263, USA. (hliu28@uncc.edu)

‡Institute of Mathematics, Academy of Mathematics and Systems Science, Chinese Academy of Sciences, Beijing 100190, P. R. China. (hpsun@amss.ac.cn)

In order to avoid the singular structures, several regularized approximate cloaking schemes are proposed in [6, 12, 13, 17, 25]. The basic idea is to introduce regularization into the singular transformation underlying the ideal cloaking, and instead of the perfect invisibility, one would consider the 'near-invisibility' depending on a regularization parameter. Our study is closely related to the one introduced in [13] for approximate cloaking in EIT, where the 'blow-up-a-point' transformation in [10, 24] is regularized to be the 'blow-up-a-small-region' transformation. The idea was further explored in [12] and [17] for the Helmholtz equation. In [17], the author imposed a homogeneous Dirichlet boundary condition at the inner edge of the cloak and showed that the 'blow-up-a-small-region' construction gives successful near-cloak. In [12], the authors introduced a special lossy-layer between the cloaked region and the cloaking region, and also showed that the 'blow-up-a-small-region' construction gives successful near-cloak. For both cloaking constructions, it was shown that the near-cloaks come, respectively, within $1/|\ln \rho|$ in 2D and ρ in 3D of the perfect cloaking, where ρ is the relative size of the small region being blown-up for the construction and plays the role of a regularization parameter. These estimates are also shown to be optimal for their constructions.

It is worth noting that if one lets the loss parameter in [12] go to infinity, this limit corresponds to the imposition of a homogeneous Dirichlet boundary condition at the inner edge of the cloak. On the other hand, the imposition of a homogeneous Dirichlet boundary condition at the inner edge of the cloak is equivalent to employing a sound-soft layer right outside the cloaked region. In this sense, the lossy layer lining in [12] is a finite realization of the sound-soft lining in [17]. We would like to emphasize that employing some special lining is necessary for the near-cloak construction, since otherwise it is shown in [12] that there exists certain resonant inclusion which defies any attempt to achieve near-cloak.

In this work, we shall impose a homogeneous Neumann boundary condition on the inner edge of the cloak, which amounts to employing a sound-hard layer right outside the cloaked region. The cloaking scheme is referred to as an *SH construction*. For the SH construction, we show that one could achieve significantly enhanced cloaking performance. Actually, it is shown that one could achieve, respectively, ρ^2 in 2D and ρ^3 in 3D within the perfect cloaking for such construction. We then develop a cloaking scheme by making use of a well-chosen lossy layer lining. The properly designed lossy-layer could be taken as a finite realization of the sound-hard lining. The cloaking scheme is referred to as an *FSH construction*. The FSH construction is shown to possess the same cloaking performance as the SH construction.

The analysis of cloaking must specify the type of exterior measurements. In [6, 12, 13], the near-cloaks are assessed in terms of boundary measurement encoded into the boundary Dirichlet-to-Neumann (DtN) map. The scattering measurement is considered for the near-cloak in [17]. In the present work, we shall assess our near-cloak construction with respect to scattering measurement encoded into the scattering amplitude. Nonetheless, by [21, 22], it can be shown, at least heuristically, that knowing the scattering amplitude amounts to knowing the boundary DtN map.

In this paper, we focus entirely on transformation-optics-approach in constructing

cloaking devices. But we would like to mention in passing the other promising cloaking schemes including the one based on anomalous localized resonance [20], and another one based on special (object-dependent) coatings [1]. It is also interesting to note a recent work in [3], where the authors implement multi-coatings to enhance the near-cloak in EIT.

The rest of the paper is organized as follows. In Section 2, we develop the cloaking scheme by employing the sound-hard lining. In Section 3, we present the cloaking scheme with a properly designed lossy layer. Section 4 is devoted to discussions on different cloaking schemes. In Section 5, we present the numerical examples.

2 Transformation acoustics and cloaking construction

Let $q \in L^\infty(\mathbb{R}^N)$ be a scalar function and $\sigma = (\sigma^{ij})_{i,j=1}^N \in \mathrm{Sym}(N)$ be a symmetric-matrix-valued function on $\mathbb{R}^N$, which is bounded in the sense that, for some constants $0 < c_0 < C_0 < \infty$,

$$c_0\xi^T\xi \leq \xi^T\sigma(x)\xi \leq C_0\xi^T\xi \tag{2.1}$$

for all $x \in \mathbb{R}^N$ and $\xi \in \mathbb{R}^N$. In acoustics, σ^{-1} and q, respectively, represent the mass density tensor and the bulk modulus of a *regular* acoustic medium. We shall denote $\{\mathbb{R}^N; \sigma, q\}$ an acoustic medium as described above. It is assumed that the inhomogeneity of the acoustic medium is compactly supported, namely, $\sigma = I$ and $q = 1$ in $\mathbb{R}^N \backslash \bar{\Omega}$ with Ω a bounded Lipschitz domain in $\mathbb{R}^N$. In $\mathbb{R}^N$, the time-harmonic acoustic wave propagation is governed by the heterogeneous Helmholtz equation

$$\mathrm{div}(\sigma\nabla u) + k^2 q u = 0, \tag{2.2}$$

where $k > 0$ represents the wave number. Stationary scattering theory is to seek a solution to (2.2) admitting the following asymptotic development

$$u(x) = e^{ix\cdot\xi} + \frac{e^{ik|x|}}{|x|^{(N-1)/2}}\left\{A\left(\frac{x}{|x|}, \frac{\xi}{|\xi|}\right) + \mathcal{O}\left(\frac{1}{|x|}\right)\right\}, \quad |x| \to \infty, \tag{2.3}$$

where $\xi = kd$ with $d \in \mathbb{S}^{N-1}$. $A(\hat{x}, d)$ with $\hat{x} := x/|x|$ is the so-called scattering amplitude. An important problem arising in practical application is to recover $\{\Omega; \sigma, q\}$ from the measurement of the corresponding scattering amplitude. In the following, for clarity and also the convenience of our subsequent study, we give a more detailed description of the scattering problem. We shall let $u^i(x) := e^{ikx\cdot d}$ denote a time-harmonic plane wave, where $d \in \mathbb{S}^{N-1}$ denotes the incident direction. Let u^{int} and u^{ext} denote the total wave fields inside and outside the inhomogeneous medium,

respectively, which satisfy the following PDE system

$$\begin{cases} \nabla\cdot(\sigma\nabla u^{int})+k^2qu^{int}=0 \quad \text{in } \Omega,\\ \Delta u^{ext}+k^2u^{ext}=0 \quad \text{in } \mathbb{R}^N\backslash\bar{\Omega},\\ u^{int}|_{\partial\Omega}=u^{ext}|_{\partial\Omega}, \quad \displaystyle\sum_{i,j=1}^{n}\nu_i\sigma^{ij}\partial_j u^{int}\Big|_{\partial\Omega}=\frac{\partial u^{ext}}{\partial\nu}\Big|_{\partial\Omega},\\ u^{ext}(x)=u^i(x)+u^s(x), \quad x\in\mathbb{R}^N\backslash\bar{\Omega},\\ \displaystyle\lim_{r\to\infty} r^{(N-1)/2}\left\{\frac{\partial u^s}{\partial r}-iku^s\right\}=0, \end{cases} \tag{2.4}$$

where $r=|x|$ for $x\in\mathbb{R}^N$. We know $u^s\in H^1_{loc}(\mathbb{R}^N)$ (see, e.g. [11, 19]) and clearly, $A(\hat{x},d)$ can be read off from the large $|x|$ asymptotics of u^s.

In this paper, we shall be concerned with the construction of a layer of cloaking medium which makes the inside scatterer invisible to scattering amplitude. To that end, we present a quick discussion on transformation acoustics. Let $\tilde{x}=F(x):\Omega\to\widetilde{\Omega}$ be a bi-Lipschitz and orientation-preserving mapping. For an acoustic medium $\{\Omega;\sigma,q\}$, we let the *push-forwarded* medium be defined as

$$\{\widetilde{\Omega};\widetilde{\sigma},\widetilde{q}\}=F_*\{\Omega;\sigma,q\}:=\{\Omega;F_*\sigma,F_*q\}, \tag{2.5}$$

where

$$\begin{aligned} \widetilde{\sigma}(\tilde{x})&=F_*\sigma(x):=\frac{1}{J}M\sigma(x)M^T|_{x=F^{-1}(\tilde{x})}\\ \widetilde{q}(\tilde{x})&=F_*q(x):=q(x)/J|_{x=F^{-1}(\tilde{x})} \end{aligned} \tag{2.6}$$

and $M=(\partial\tilde{x}_i/\partial x_j)_{i,j=1}^n$, $J=\det(M)$. Then $u\in H^1(\Omega)$ solves the Helmholtz equation

$$\nabla\cdot(\sigma\nabla u)+k^2qu=0 \quad \text{on } \Omega,$$

if and only if the pull-back field $\widetilde{u}=(F^{-1})^*u:=u\circ F^{-1}\in H^1(\widetilde{\Omega})$ solves

$$\widetilde{\nabla}\cdot(\widetilde{\sigma}\widetilde{\nabla}\widetilde{u})+k^2\widetilde{q}\widetilde{u}=0.$$

We have made use of ∇ and $\widetilde{\nabla}$ to distinguish the differentiations respectively in x- and $\tilde{x}$-coordinates. We refer to [12, 17] for a proof of this invariance.

We are in a position to construct the cloaking device. In the sequel, let $D\Subset\Omega$ be a Lipschitz domain such that $\Omega\backslash\bar{D}$ is connected. W.L.O.G., we assume that D contains the origin. Let $\rho>0$ be sufficiently small and $D_\rho:=\{\rho x;x\in D\}$. Suppose

$$F_\rho:\bar{\Omega}\backslash D_\rho\to\bar{\Omega}\backslash D, \tag{2.7}$$

which is a bi-Lipschitz and orientation-preserving mapping, and $F_\rho|_{\partial\Omega}=\text{Identity}$. A celebrated example of such blow-up mapping is given by

$$y=F_\rho(x):=\left(\frac{R_1-\rho}{R_2-\rho}R_2+\frac{R_2-R_1}{R_2-\rho}|x|\right)\frac{x}{|x|}, \quad \rho<R_1<R_2 \tag{2.8}$$

which blows-up the central ball B_ρ to B_{R_1} within B_{R_2}. Now, we set

$$\{\Omega\backslash\bar{D}; \sigma_c^\rho, q_c^\rho\} = (F_\rho)_*\{\Omega\backslash\bar{D}_\rho; I, 1\}. \tag{2.9}$$

Let $M \Subset D$ represent the cloaked region. Then we claim the following construction gives a near-cloaking device

$$\{\mathbb{R}^N; \sigma, q\} = \begin{cases} \{I, 1\} & \text{in } \mathbb{R}^N\backslash\bar{\Omega}; \\ \{\sigma_c^\rho, q_c^\rho\} & \text{in } \Omega\backslash\bar{D}; \\ \text{a sound-hard layer} & \text{in } D\backslash M; \\ \text{arbitrary target object} & \text{in } M. \end{cases} \tag{2.10}$$

In (2.10), by a sound-hard layer we mean a layer of material which prevents acoustic wave from penetrating inside and the normal velocity of the underlying wave field vanishes on the exterior boundary of the layer. The wave equation governing the wave scattering corresponding to the cloaking device constructed in (2.10) is

$$\begin{cases} \nabla \cdot (\sigma \nabla u) + k^2 q u = 0 \quad \text{in } \mathbb{R}^N\backslash\bar{D}, \\ \displaystyle\sum_{i,j=1}^{N} (\sigma_c^\rho)^{ij} \nu_i \partial_j u = 0 \quad \text{on } \partial D, \end{cases} \tag{2.11}$$

where $\nu = (\nu_i)_{i=1}^N$ is the exterior unit normal vector to ∂D. In the following, we shall let $\mathcal{A}(\hat{x}, d)$ denote the scattering amplitude to the PDE system (2.11) corresponding to the cloaking device. Let

$$F = F_\rho \quad \text{on } \Omega\backslash\bar{D}_\rho; \quad \text{Identity on } \mathbb{R}^N\backslash\Omega.$$

Set $v = F^* u \in H^1_{loc}(\mathbb{R}^N\backslash\bar{D}_\rho)$ and $v^s(x) := v(x) - e^{ikx\cdot d}$. By transformation acoustics, together with straightforward calculations, one can show that

$$\begin{cases} (\Delta + k^2) v = 0 \quad \text{in } \mathbb{R}^N\backslash\bar{D}_\rho, \\ \left.\dfrac{\partial v}{\partial \nu}\right|_{\partial D_\rho} = 0, \\ v(x) = v^s(x) + e^{ix\cdot\xi} \quad x \in \mathbb{R}^N\backslash\bar{D}_\rho, \\ \displaystyle\lim_{r\to\infty} r^{(N-1)/2} \left\{ \frac{\partial v^s}{\partial r} - ikv^s \right\} = 0. \end{cases} \tag{2.12}$$

In terms of the terminologies in [17], (2.11) describes the scattering in the physical space and (2.12) describes the scattering in the virtual space. Since $v = u$ in $\mathbb{R}^N\backslash\bar{\Omega}$, we see the scattering in the physical space is the same as that in the virtual space. That is, $\mathcal{A}(\hat{x}, d)$ could also be read off from the large $|x|$ asymptotics of v^s. Next, we give one of the main results of this paper, which justifies the near-invisibility of the above construction.

Theorem 2.1. *There exists $\rho_0 > 0$ such that when $\rho < \rho_0$ the scattering amplitude $\mathcal{A}(\hat{x}, d)$ to (2.12) satisfies*

$$|\mathcal{A}(\hat{x}, d)| \leq C\rho^N, \quad \hat{x}, d \in \mathbb{S}^{N-1}, \tag{2.13}$$

where C is a constant dependent only on k, ρ_0 and D, but completely independent of ρ.

Proof. In order to ease the exposition, we shall only prove the theorem for $N = 2, 3$. But we would like to emphasize that for $N > 3$, the proof follows by completely similar arguments.

Let

$$G(x) = \frac{i}{4}\left(\frac{k}{2\pi|x|}\right)^{(N-2)/2} H^{(1)}_{(N-2)/2}(k|x|) \tag{2.14}$$

be the outgoing Green's function. By Green's representation, we know for $x \in \mathbb{R}^N \backslash \bar{D}_\rho$

$$\begin{aligned} v^s(x) =& \int_{\partial D_\rho} \left\{ \frac{\partial G(x-y)}{\partial \nu(y)} v^s(y) - G(x-y) \frac{\partial v^s(y)}{\partial \nu(y)} \right\} ds(y) \\ =& (\mathcal{K}v^s)(x) + g(x), \end{aligned} \tag{2.15}$$

where we have set

$$(\mathcal{K}v^s)(x) := \int_{\partial D_\rho} \frac{\partial G(x-y)}{\partial \nu(y)} v^s(y)\, ds(y), \tag{2.16}$$

$$g(x) := -\int_{\partial D_\rho} G(x-y) \frac{\partial v^s(y)}{\partial \nu(y)}\, ds(y). \tag{2.17}$$

Clearly, $v^s(x)|_{\partial D_\rho} \in H^{1/2}(\partial D_\rho)$. By the jump properties of the double-layer potential operator $\mathcal{K}$ (cf. [19]), we have from (2.15)

$$\frac{1}{2} v^s(x) = (\mathcal{K}v^s)(x) + g(x), \quad x \in \partial D_\rho. \tag{2.18}$$

Let $x' = x/\rho$, then (2.18) is read as

$$\frac{1}{2} v^s(\rho x') = (\mathcal{K}v^s)(\rho x') + g(\rho x'), \quad x' \in \partial D. \tag{2.19}$$

Next, we claim

$$\|g(\rho\, \cdot)\|_{L^2(\partial D)} \leq C\rho, \tag{2.20}$$

where C remains uniform as $\rho \to 0^+$. In the sequel, we shall make use of the following asymptotic developments of the 2D $G(x)$ (cf. [5]),

$$G(x) = -\frac{1}{2\pi} \ln|x| + \frac{i}{4} - \frac{1}{2\pi} \ln\frac{k}{2} - \frac{E}{2\pi} + \mathcal{O}\left(|x|^2 \ln|x|\right) \tag{2.21}$$

for $|x| \to 0$, where E is the Euler's constant. Moreover, we know that

$$G(x) = \frac{e^{ik|x|}}{4\pi|x|} \quad \text{when } N = 3. \tag{2.22}$$

In order to prove (2.20), we first assume $x \in \partial D_{t\rho}$ with $1 < t \leq 2$. Then by Green's formula, we have

$$\begin{aligned} &\int_{\partial D_\rho} G(x-y) \frac{\partial e^{iky\cdot d}}{\partial \nu(y)}\, ds(y) \\ =&\int_{D_\rho} \Delta_y e^{iky\cdot d} G(x-y)\, dy + \int_{D_\rho} \nabla_y G(x-y)\cdot \nabla_y e^{iky\cdot d}\, dy \\ =&-k^2 \int_{D_\rho} e^{iky\cdot d} G(x-y)\, dy + \int_{D_\rho} \nabla_y G(x-y)\cdot \nabla_y e^{iky\cdot d}\, dy. \end{aligned} \tag{2.23}$$

Using (2.21) and (2.22), we have for $x' \in D_t$

$$\begin{aligned} |g_1(\rho x')| &= k^2 \Big| \int_{D_\rho} e^{iky\cdot d} G(\rho x' - y)\, dy \Big| \\ &\leq k^2 \int_D |G(\rho(x'-y'))\rho^n dy'|. \end{aligned}$$

By the mapping properties of volume potential operator, one has

$$|g_1(x)|_{C(\partial D_{t\rho})} \leq C\rho, \tag{2.24}$$

where C is independent of ρ and t. In like manner, one can show that

$$|g_2(x)|_{C(\partial D_{t\rho})} = \Big| \int_{D_\rho} \nabla_y G(x-y)\cdot \nabla_y e^{iky\cdot d}\, dy \Big|_{C(\partial D_{t\rho})} \leq C\rho. \tag{2.25}$$

By (2.24) and (2.25), we see

$$|g(x)|_{C(D_{t\rho})} \leq C\rho. \tag{2.26}$$

Next, by the mapping property of single-layer potential operator, we know

$$g(x)|_{\partial D_\rho} = \lim_{t\to 1^+} \left(g(x)|_{\partial D_{t\rho}} \right), \tag{2.27}$$

which together with (2.26) implies (2.20).

We proceed to the integral equation (2.18). First, by using change of variables in integrals, it is straightforward to show that

$$(\mathcal{K} v^s)(\rho x') = (\mathcal{K}_0 v^s(\rho\,\cdot))(\rho x') + (R v^s(\rho\,\cdot))(\rho x'), \quad x' \in \partial D, \tag{2.28}$$

where $\mathcal{K}_0$ is an integral operator with the kernel given by

$$G_0(x-y) = \begin{cases} -\dfrac{1}{2\pi} \ln|x-y| & N = 2, \\ \dfrac{1}{4\pi} \dfrac{1}{|x-y|} & N = 3, \end{cases}$$

which is the fundamental solution to $-\Delta$; and R satisfies

$$\|R\|_{\mathcal{L}(L^2(D),L^2(D))} \lesssim \begin{cases} \rho \ln \rho & \text{when } N=2; \\ \rho & \text{when } N=3. \end{cases} \tag{2.29}$$

Hence, the integral equation (2.19) can be reformulated as

$$\left[(\frac{1}{2} I - \mathcal{K}_0 - R) v^s(\rho\, \cdot) \right] (\rho x') = g(\rho x') \quad x' \in D. \tag{2.30}$$

By the well-known result in [27], $I - \frac{1}{2}\mathcal{K}_0$ is invertible from $L^2(\partial D)$ to $L^2(\partial D)$. Then, by using (2.20), we have from (2.30) that

$$\|v^s(\rho\, \cdot)\|_{L^2(\partial D)} \leq C \|g(\rho\, \cdot)\|_{L^2(\partial D)} \leq C\rho. \tag{2.31}$$

Noting $\|v^s(\cdot)\|_{L^2(\partial D_\rho)} = \rho^{(N-1)/2} \|v^s(\rho\, \cdot)\|_{L^2(\partial D)}$, we further have from (2.31) that

$$\|v^s\|_{L^2(\partial D_\rho)} \leq \begin{cases} C\rho^{3/2} & N=2, \\ C\rho^2 & N=3. \end{cases} \tag{2.32}$$

Finally, by letting $|x| \to \infty$ in (2.15), we have

$$\mathcal{A}(\hat{x}, d) = \gamma \int_{\partial D_\rho} \left[\frac{\partial e^{-ik\hat{x}\cdot y}}{\partial \nu(y)} v^s(y) + e^{-ik\hat{x}\cdot y} \frac{\partial e^{iky\cdot d}}{\partial \nu(y)} \right] \, ds(y), \tag{2.33}$$

where $\gamma = e^{i\frac{\pi}{4}}/\sqrt{8\pi k}$ when $N=2$, and $\gamma = 1/4\pi$ when $N=3$. By using (2.32) and the Schwarz inequality in (2.33), we have

$$\left| \int_{\partial D_\rho} \frac{\partial e^{-ik\hat{x}\cdot y}}{\partial \nu(y)} v^s(y) \, ds(y) \right| \leq C\rho^N. \tag{2.34}$$

By Green's formula, we have

$$\begin{aligned} & \left| \int_{\partial D_\rho} e^{-ik\hat{x}\cdot y} \frac{\partial e^{iky\cdot d}}{\partial \nu(y)} \, ds(y) \right| \\ =& \left| \int_{D_\rho} (\Delta e^{iky\cdot d}) e^{-ik\hat{x}\cdot y} \, dy + \int_{D_\rho} \nabla e^{iky\cdot d} \cdot \nabla e^{-ik\hat{x}\cdot y} \, dy \right| \\ =& |k^2 (d\cdot\hat{x} - 1) \int_{D_\rho} e^{ik(d-\hat{x})\cdot y} \, dy| \\ \leq& C\rho^N. \end{aligned} \tag{2.35}$$

By (2.33), (2.34) and (2.35), we have (2.13).

The proof is completed.

□

By Theorem 2.1, we know the construction (2.10) gives a near-invisibility cloaking within ρ^N of the perfect cloaking. For a special case by taking $D_\rho = B_\rho$, namely, the central ball of radius $\rho > 0$, using wave functions expansion, one can show (cf. [18])

$$\mathcal{A}(\hat{x}, d) = -e^{-i\frac{\pi}{4}}\sqrt{\frac{2}{\pi k}}\left[\frac{J_0'(k\rho)}{H_0^{(1)'}(k\rho)} + 2\sum_{n=1}^{\infty}\frac{J_n'(k\rho)}{H_n^{(1)'}(k\rho)}\cos n\theta\right] \tag{2.36}$$

in $\mathbb{R}^2$, where $\theta = \angle(\hat{x}, d)$; and

$$\mathcal{A}(\hat{x}, d) = \frac{i}{k}\sum_{n=0}^{\infty}(2n+1)\frac{j_n'(k\rho)}{h_n^{(1)'}(k\rho)}P_n(\cos\theta) \tag{2.37}$$

in $\mathbb{R}^3$, where P_n is the Legendre polynomial of degree n. By the asymptotic developments of spherical Bessel functions (cf. [18]), one has from (2.37)

$$\mathcal{A}(\hat{x}, d) = \frac{i}{k}\left(\frac{\cos\theta}{2} - \frac{1}{3}\right)(k\rho)^3 + \mathcal{O}((k\rho)^5). \tag{2.38}$$

Similarly, by (2.36) one can show that in $\mathbb{R}^2$,

$$\mathcal{A}(\hat{x}, d) = -e^{-i\frac{\pi}{4}}\sqrt{\frac{2\pi}{k}}\left(\frac{\cos\theta}{2} - \frac{1}{4}\right)(k\rho)^2 + \mathcal{O}((k\rho)^4). \tag{2.39}$$

By (2.38) and (2.39), it is readily seen that the estimates in Theorem 2.1 are optimal for full scattering measurements, namely, $\hat{x} \in \mathbb{S}^{N-1}$ and $d \in \mathbb{S}^{N-1}$. Nevertheless, it is interesting to note from (2.38) and (2.39) that for some specific scattering measurements, e.g., $\mathcal{A}(\hat{x}, d)$ with $\angle(\hat{x}, d) = \pm\arccos\frac{2}{3}$ in 3D, and with $\angle(\hat{x}, d) = \pm\frac{\pi}{3}$ in 2D, one would have even more enhanced invisibility cloaking effects. Physically speaking, the cloaking effect would be stronger in the backward scattering region, i.e. $|\angle(\hat{x}, d)| > \pi/2$, than that in the forward scattering region, i.e. $|\angle(\hat{x}, d)| > \pi/2$. This could be partly seen from (2.33)–(2.35), and (2.38)–(2.39).

3 Near-cloak construction with a lossy layer

In this section, we shall develop a lossy approximate cloaking scheme. To that end, we first introduce the following transformation $T : \mathbb{R}^N \to \mathbb{R}^N$,

$$y = T(x) := \begin{cases} x & \text{for } x \in \mathbb{R}^N\backslash\bar{\Omega}, \\ F_\rho(x) & \text{for } x \in \Omega\backslash D_\rho, \\ \frac{x}{\rho} & \text{for } x \in D_\rho, \end{cases} \tag{3.1}$$

where F_ρ is given in (2.7). Let

$$\{\mathbb{R}^N; \sigma, q\} = \begin{cases} I, 1 & \text{in } \mathbb{R}^N\backslash\Omega, \\ T_*I, T_*1 & \text{in } \Omega\backslash D, \\ T_*\sigma_l, T_*q_l & \text{in } D\backslash D_{1/2}, \\ \sigma_a', q_a' & \text{in } D_{1/2}, \end{cases} \tag{3.2}$$

be the cloaking device in the physical space. Here, $\{D_{1/2}; \sigma'_a, q'_a\}$ is an arbitrary but regular medium, which represents the target object being cloaked; and

$$\{D_\rho \backslash D_{\rho/2}; \sigma_l, q_l\} \tag{3.3}$$

is a lossy layer whose parameters shall be specified in the following. Similar to our earlier argument in Section 3, by transformation acoustics we see that the scattering amplitude in the physical space corresponding to the cloaking device is the same as the one in the virtual space. In the virtual space, the wave scattering is governed by the following PDE system

$$\begin{cases} (\Delta + k^2)u = 0 & \text{in } \mathbb{R}^N \backslash \bar{D}_\rho, \\ \nabla \cdot (\sigma_l \nabla u) + k^2 q_l u = 0 & \text{in } D_\rho \backslash \bar{D}_{\rho/2}, \\ \nabla \cdot (\sigma_a \nabla u) + k^2 q_a u = 0 & \text{in } D_{\rho/2}, \end{cases} \tag{3.4}$$

where

$$\{D_{\rho/2}; \sigma_a, q_a\} = (T^{-1})_* \{D_{1/2}; \sigma'_a, q'_a\} \tag{3.5}$$

is arbitrary but regular; and $u \in H^1_{loc}(\mathbb{R}^N)$ satisfies

$$\begin{aligned} & u(x) = e^{ikx\cdot d} + u^s(x) \quad \text{for } x \in \mathbb{R}^N \backslash D_\rho, \\ & \lim_{r\to\infty} r^{(N-1)/2} \left\{ \frac{\partial u^s}{\partial r} - iku^s \right\} = 0. \end{aligned}$$

We shall choose

$$\sigma_l = C\rho^{2+2\delta} I \quad \text{and} \quad q_l = a + ib \tag{3.6}$$

with C, δ, a, b some fixed positive constants in our construction. We shall show that it will yield an enhanced approximate cloaking scheme. However, the proof for the general case with general geometry and arbitrary cloaked contents is rather technical and lengthy, which we choose to extend to full details in our forthcoming paper [15]. In this section, we shall consider the special case with spherical geometry and uniform cloaked contents. In the sequel, we let $D_\rho = B_\rho$ and, σ'_a and q'_a be arbitrary positive constants but independent of ρ. With a bit abusing of notation, we shall also write

$$\sigma_l = C\rho^{2+2\delta}.$$

By (3.5), one can show by direct calculations that in the virtual space

$$\sigma_a, q_a = \begin{cases} \sigma'_a, \frac{q'_a}{\rho^2} & \text{in } D_{\rho/2} \text{ when } N = 2 \\ \frac{\sigma'_a}{\rho}, \frac{q'_a}{\rho^3} & \text{in } D_{\rho/2} \text{ when } N = 3 \end{cases}.$$

For the PDE system (3.4), we let $u = u_0$ in $\mathbb{R}^N \backslash \bar{D}_\rho$, $u = u_2$ in $D_\rho \backslash \bar{D}_{\rho/2}$ and $u = u_{int}$ in $D_{\rho/2}$. By transmission conditions, we have

$$u_2 = u_0 \quad \text{and} \quad \sigma_l \frac{\partial u_2}{\partial \nu} = \frac{\partial u_0}{\partial \nu} \quad \text{on } \partial D_\rho, \tag{3.7}$$

and

$$u_2 = u_{int} \quad \text{and} \quad \sigma_l \frac{\partial u_2}{\partial \nu} = \sigma_a \frac{\partial u_{int}}{\partial \nu} \quad \text{on } \partial D_{\rho/2}. \tag{3.8}$$

Set $\tilde{k} = k\sqrt{\frac{q_l}{\sigma_l}}$ and $k_2 = k\sqrt{\frac{q_a}{\sigma_a}}$. We choose the complex branch of $\tilde{k}$ such that $\Im(\tilde{k}) > 0$.

We first consider the 2D case. By [5], one has the following series expansions

$$\begin{cases} u_0(x) = e^{ikx\cdot d} + u^s = \sum\limits_{n=-\infty}^{\infty} i^n J_n(k|x|)e^{in\theta} + \sum\limits_{n=-\infty}^{\infty} d_n H_n^{(1)}(k|x|)e^{in\theta}, \\ u_2(x) = \sum\limits_{n=-\infty}^{\infty} a_n J_n(\tilde{k}|x|)e^{in\theta} + \sum\limits_{n=-\infty}^{\infty} b_n H_n^{(1)}(\tilde{k}|x|)e^{in\theta}, \\ u_{int} = \sum\limits_{n=-\infty}^{\infty} c_n J_n(k_2|x|)e^{in\theta}. \end{cases} \tag{3.9}$$

By (3.7) and (3.9), we have

$$\begin{cases} a_n J_n(\tilde{k}\rho) + b_n H_n^{(1)}(\tilde{k}\rho) = i^n J_n(k\rho) + d_n H_n^{(1)}(k\rho) \\ \sigma_l[a_n \tilde{k} J_n'(\tilde{k}\rho) + b_n \tilde{k} H_n^{(1)'}(\tilde{k}\rho)] = i^n k J_n'(k\rho) + d_n k H_n^{(1)'}(k\rho). \end{cases} \tag{3.10}$$

In like manner, by (3.8) and (3.9) we have

$$\begin{cases} a_n J_n(\tilde{k}\rho/2) + b_n H_n(1)(\tilde{k}\rho/2) = c_n J_n(k_2\rho/2) \\ \sigma_l[a_n \tilde{k} J_n'(\tilde{k}\rho/2) + b_n \tilde{k} H_n^{(1)'}(\tilde{k}\rho/2)] = \sigma_a c_n k_2 J_n'(k_2\rho/2). \end{cases} \tag{3.11}$$

Here $J_n'(\tilde{k}\rho) = \frac{dJ_n(z)}{dz}|_{z=\tilde{k}\rho}$ and $J_n'(\tilde{k}\rho/2) = \frac{dJ_n(z)}{dz}|_{z=\tilde{k}\rho/2}$. $H_n^{(1)'}(\tilde{k}\rho)$, $H_n^{(1)'}(\tilde{k}\rho/2)$, $J_n'(k\rho)$, $H_n^{(1)'}(k\rho)$, $J_n'(k_2\rho/2)$, $H_n^{(1)'}(k_2\rho/2)$ are understood in the same sense. By letting $C_0 = 1/\sqrt{\sigma_l q_l}$ and $A = \sqrt{q_a\sigma_a} = \sqrt{q_a'\sigma_a'}/\rho$, $k_2 = \frac{k}{\rho}\sqrt{\frac{q_a'}{\sigma_a'}}$, (3.10) and (3.11) are read as

$$\begin{cases} a_n J_n(\tilde{k}\rho) + b_n H_n^{(1)}(\tilde{k}\rho) = i^n J_n(k\rho) + d_n H_n^{(1)}(k\rho) \\ [a_n J_n'(\tilde{k}\rho) + b_n H_n^{(1)'}(\tilde{k}\rho)] = C_0[i^n J_n'(k\rho) + d_n H_n^{(1)'}(k\rho)], \end{cases} \tag{3.12}$$

and

$$\begin{cases} a_n J_n(\tilde{k}\rho/2) + b_n H_n^{(1)}(\tilde{k}\rho/2) = c_n J_n(k_2\rho/2) \\ [a_n J_n'(\tilde{k}\rho/2) + b_n H_n^{(1)'}(\tilde{k}\rho/2)] = C_0 A c_n J_n'(k_2\rho/2). \end{cases} \tag{3.13}$$

Noting $k_2\rho = k\sqrt{q_a'/\sigma_a'}$, if $J_n(k_2\rho/2) \neq 0$ then by direct calculations, we have from (3.13)

$$c_n = \frac{a_n J_n(\tilde{k}\rho/2) + b_n H_n^{(1)}(\tilde{k}\rho/2)}{J_n(k_2\rho/2)}$$

and

$$b_n = -\frac{J_n'(\tilde{k}\rho/2) - C_0 A \frac{J_n'(k_2\rho/2)}{J_n(k_2\rho/2)} J_n(\tilde{k}\rho/2)}{H_n^{(1)'}(\tilde{k}\rho/2) - C_0 A \frac{J_n'(k_2\rho/2)}{J_n(k_2\rho/2)} H_n^{(1)}(\tilde{k}\rho/2)} a_n. \tag{3.14}$$

In case $J_n(k_2\rho/2)=0$, we have from the first equation in (3.13) that

$$b_n=-\frac{J_n(\tilde{k}\rho/2)}{H_n^{(1)}(\tilde{k}\rho/2)}a_n. \tag{3.15}$$

Let Υ_0 denote the fraction in (3.14) or (3.15) and hence $b_n=\Upsilon_0 a_n$. Plugging b_n into (3.12), we have by straightforward calculations

$$a_n=\frac{i^nJ_n(k\rho)+d_nH_n^{(1)}(k\rho)}{J_n(\tilde{k}\rho)+\Upsilon_0H_n^{(1)}(\tilde{k}\rho)},$$

and

$$d_n=-\frac{i^nJ_n'(k\rho)-\frac{1}{C_0}\frac{J_n'(\tilde{k}\rho)+\Upsilon_0H_n^{(1)\prime}(\tilde{k}\rho)}{J_n(\tilde{k}\rho)+\Upsilon_0H_n^{(1)}(\tilde{k}\rho)}i^nJ_n(k\rho)}{H_n^{(1)\prime}(k\rho)-\frac{1}{C_0}\frac{J_n'(\tilde{k}\rho)+\Upsilon_0H_n^{(1)\prime}(\tilde{k}\rho)}{J_n(\tilde{k}\rho)+\Upsilon_0H_n^{(1)}(\tilde{k}\rho)}H_n^{(1)}(k\rho)}. \tag{3.16}$$

We next investigate the asymptotic development of

$$\mathcal{H}(\sigma_l,\rho):=\frac{1}{C_0}\frac{J_n'(\tilde{k}\rho)+\Upsilon_0H_n^{(1)\prime}(\tilde{k}\rho)}{J_n(\tilde{k}\rho)+\Upsilon_0H_n^{(1)}(\tilde{k}\rho)}=\frac{\frac{1}{C_0}\frac{J_n'(\tilde{k}\rho)}{J_n(\tilde{k}\rho)}+\frac{1}{C_0}\Upsilon_0\frac{H_n^{(1)\prime}(\tilde{k}\rho)}{J_n(\tilde{k}\rho)}}{1+\Upsilon_0\frac{H_n^{(1)}(\tilde{k}\rho)}{J_n(\tilde{k}\rho)}}. \tag{3.17}$$

Clearly, we only need study the asymptotic behaviors of $\frac{1}{C_0}\frac{J_n'(\tilde{k}\rho)}{J_n(\tilde{k}\rho)}$, $\frac{1}{C_0}\Upsilon_0\frac{H_n^{(1)\prime}(\tilde{k}\rho)}{J_n(\tilde{k}\rho)}$ and $\Upsilon_0\frac{H_n^{(1)}(\tilde{k}\rho)}{J_n(\tilde{k}\rho)}$. We note the following fact due to (3.6),

$$\Re(\tilde{k}\rho)\to+\infty\quad\text{and}\quad\Im(\tilde{k}\rho)\to+\infty\quad\text{as}\quad\rho\to0^+,$$

which implies the following asymptotic developments for $z=\tilde{k}\rho$ (see formulas 9.2.1, 9.2.3 in [2]),

$$\begin{cases}J_n(z)\sim\sqrt{\frac{2}{\pi z}}\cos(z-\frac{n\pi}{2}-\frac{\pi}{4})+e^{|\Im(z)|}\mathcal{O}(|z|^{-1}), & |\arg z|<\pi\\ H_n^{(1)}(z)\sim\sqrt{\frac{2}{\pi z}}e^{i(z-\frac{n\pi}{2}-\frac{\pi}{4})}, & -\pi<\arg z<2\pi\end{cases} \tag{3.18}$$

We also note the following recurrence relation (see formula 9.1.27 in [2]) for the subsequent use,

$$\mathcal{B}_n'(z)=\frac{n}{z}\mathcal{B}_n(z)-\mathcal{B}_{n+1}(z) \tag{3.19}$$

where $\mathcal{B}_n(z)=J_n(z)$ or $H_n^{(1)}(z)$. Since $J_n(z)=(-1)^nJ_n(z)$ and $H_n^{(1)}(z)=(-1)^nH_{-n}^{(1)}(z)$ (see formula 9.1.5 in [2]), we only need consider the case with $n\geq0$ in the sequel.

Noting $\cos(z)=\frac{e^{iz}+e^{-iz}}{2}$, by (3.18) we further have as $\Re(z),\Im(z)\to\infty$

$$\begin{cases}J_n(z)\sim\sqrt{\frac{1}{2\pi z}}e^{|\Im(z)|}e^{i(-\Re(z)+\frac{n\pi}{2}+\frac{\pi}{4})}, & |\arg z|<\pi\\ H_n^{(1)}(z)\sim\sqrt{\frac{2}{\pi z}}e^{-\Im(z)}e^{i(\Re(z)-\frac{n\pi}{2}-\frac{\pi}{4})}, & -\pi<\arg z<2\pi\\ |H_n^{(1)\prime}(z)|\sim\sqrt{\frac{2}{\pi|z|}}e^{-\Im(z)}, & -\pi<\arg z<2\pi\end{cases} \tag{3.20}$$

It is remarked that the third equation in (3.20) is obtained by using the recurrence relation (3.19). Hence we see for $z = \tilde{k}\rho$, $J_n(z)$ blows up exponentially, while $H_n^{(1)}(z)$ decreases exponentially as $\rho \to 0^+$. In the sequel, we let $\sqrt{a+ib} = \alpha + i\beta$ with $\alpha, \beta > 0$. For $\frac{1}{C_0}\frac{J_n'(\tilde{k}\rho)}{J_n(\tilde{k}\rho)}$, as $\rho \to 0^+$, by (3.20) we have

$$\frac{1}{C_0}\frac{J_n'(\tilde{k}\rho)}{J_n(\tilde{k}\rho)} = \frac{1}{C_0}\frac{\frac{n}{\tilde{k}\rho}J_n(\tilde{k}\rho) - J_{n+1}(\tilde{k}\rho)}{J_n(\tilde{k}\rho)} \sim -e^{i\pi/2}\frac{1}{C_0} = -e^{i\pi/2}(\alpha+i\beta)\sqrt{\sigma_l} \to +0. \tag{3.21}$$

For $\Upsilon_0\frac{H_n^{(1)}(\tilde{k}\rho)}{J_n(\tilde{k}\rho)}$, if Υ_0 is the fraction in (3.14), then we have

$$\begin{aligned}
\Upsilon_0\frac{H_n^{(1)}(\tilde{k}\rho)}{J_n(\tilde{k}\rho)} &= -\frac{J_n'(\tilde{k}\rho/2) - C_0A\frac{J_n'(k_2\rho/2)}{J_n(k_2\rho/2)}J_n(\tilde{k}\rho/2)}{H_n^{(1)'}(\tilde{k}\rho/2) - C_0A\frac{J_n'(k_2\rho/2)}{J_n(k_2\rho/2)}H_n^{(1)}(\tilde{k}\rho/2)}\frac{H_n^{(1)}(\tilde{k}\rho)}{J_n(\tilde{k}\rho)} \\
&= -\frac{J_n'(\tilde{k}\rho/2) - C_0A\frac{J_n'(k_2\rho/2)}{J_n(k_2\rho/2)}J_n(\tilde{k}\rho/2)}{J_n(\tilde{k}\rho)}\frac{H_n^{(1)}(\tilde{k}\rho)}{H_n^{(1)'}(\tilde{k}\rho/2) - C_0A\frac{J_n'(k_2\rho/2)}{J_n(k_2\rho/2)}H_n^{(1)}(\tilde{k}\rho/2)} \\
&:= \mathcal{Y}_1 \times \mathcal{Y}_2.
\end{aligned} \tag{3.22}$$

By straightforward asymptotic analysis, one can show as $\rho \to 0^+$

$$\begin{aligned}
|\mathcal{Y}_1| &= \left|\frac{J_n'(\tilde{k}\rho/2) - C_0A\frac{J_n'(k_2\rho/2)}{J_n(k_2\rho/2)}J_n(\tilde{k}\rho/2)}{J_n(\tilde{k}\rho)}\right| \\
&\sim \left|\left(e^{i\pi/2} - C_0A\frac{J_n'(k_2\rho/2)}{J_n(k_2\rho/2)}\right)\frac{J_n(\tilde{k}\rho/2)}{J_n(\tilde{k}\rho)}\right| \\
&\le \widetilde{C}\left(1 + (n+1)|\alpha+i\beta|\rho^{-2-\delta}\right)\left|e^{-\frac{\beta}{2}k\rho^{-\delta}}\right|,
\end{aligned} \tag{3.23}$$

where $\widetilde{C}$ is a constant independent of ρ. That is, $|\mathcal{Y}_1|$ decreases to 0 more quickly than ρ^r for any $r > 0$. Similarly, one can show that $|\mathcal{Y}_2|$ decreases to 0 more quickly than ρ^r for any $r > 0$. Furthermore, if Υ_0 is the fraction in (3.15), by completely similar arguments one can show that $\Upsilon_0\frac{H_n^{(1)}(\tilde{k}\rho)}{J_n(\tilde{k}\rho)}$ also decays more quickly than ρ^r for any $r > 0$. Hence, by (3.17)–(3.23) and $\sigma_l = \rho^{2+2\delta}$, we have

$$\mathcal{H}(\sigma_l, \rho) \sim \frac{1}{C_0}\frac{J_n'(\tilde{k}\rho)}{J_n(\tilde{k}\rho)} \sim -e^{i\pi/2}\frac{1}{C_0} = -e^{i\pi/2}(\alpha+i\beta)\rho^{1+\delta} \quad \text{as} \quad \rho \to 0^+. \tag{3.24}$$

Now, by (3.24) and (3.16) we have

$$d_n = -\frac{i^nJ_n'(k\rho) + e^{i\pi/2}(\alpha+\beta i)\rho^{1+\delta}i^nJ_n(k\rho)}{H_n^{(1)'}(k\rho) + e^{i\pi/2}(\alpha+\beta i)\rho^{1+\delta}H_n^{(1)}(k\rho)}. \tag{3.25}$$

Using the asymptotic developments of Bessel functions and their derivatives (cf. [18]), we further have

$$\begin{cases} d_0 \sim -\dfrac{-k\rho/2 + e^{i\pi/2}(\alpha+i\beta)\rho^{1+\delta}}{i\frac{2}{\pi k\rho} + e^{i\pi/2}(\alpha+i\beta)\rho^{1+\delta}\frac{2i}{\pi} ln(k\rho/2)}, \quad n=0, \\ d_n \sim -\dfrac{\frac{i^n n(k\rho)^{n-1}}{2^n\Gamma(n+1)} + e^{i\pi/2}(\alpha+i\beta)\rho^{1+\delta} i^n \frac{(k\rho)^n}{2^n\Gamma(n+1)}}{\frac{i2^n n!}{\pi(k\rho)^{n+1}} - e^{i\pi/2}(\alpha+i\beta)\rho^{1+\delta} i\frac{2^n(n-1)!}{\pi(k\rho)^n}}, \ n\in\mathbb{N}, \end{cases} \tag{3.26}$$

which imply

$$\begin{cases} d_0 \sim \mathcal{O}(\rho^2), \quad n=0 \\ d_n \sim \mathcal{O}(\rho^{2n}), \quad n\in\mathbb{N} \end{cases} \tag{3.27}$$

and

$$\begin{aligned} \left| d_0 - \left[-\frac{J_0'(k\rho)}{H_0^{(1)'}(k\rho)} \right] \right| &\leq \pi k|\alpha+i\beta|\rho^{2+\delta}, \\ \left| d_n - \left[-\frac{i^n J_n'(k\rho)}{H_n^{(1)'}(k\rho)} \right] \right| &\leq \frac{4\pi|\alpha+i\beta|}{k^{1+\delta}} \frac{1}{(2^n n!)^2} (k\rho)^{2n+2+\delta}. \end{aligned} \tag{3.28}$$

Since

$$u^s(x) = \sum_{n=-\infty}^{\infty} d_n H_n^{(1)}(k|x|)e^{in\theta}, \tag{3.29}$$

by taking $|x| \to +\infty$, together with (3.27), one has by direct calculations that the corresponding scattering amplitude satisfies

$$|\mathcal{A}(\hat{x}, d)| \leq C\rho^2, \tag{3.30}$$

where C is a positive constant that remains uniform as $\rho \to 0^+$. That is, the construction (3.2) gives an near-cloaking device within ρ^2 of the ideal cloaking.

Now, we look into the series representation of the scattered wave filed (3.29). If D_ρ is a sound-hard obstacle, the scattered wave corresponding to $e^{ikx\cdot d}$ is given by (see eqn. (3.19) in [18])

$$\tilde{u}^s(x) = -\sum_{n=-\infty}^{\infty} \frac{i^n J_n'(k\rho)}{H_n^{(1)'}(k\rho)} H_n^{(1)}(kx)e^{in\theta}. \tag{3.31}$$

By (3.28), (3.29) and (3.31), one has by direct verifications that for ρ sufficiently small

$$|u^s(x) - \tilde{u}^s(x)| \leq C\rho^{2+\delta} \tag{3.32}$$

for any $x \in \mathbb{R}^2\backslash\bar{B}_{\epsilon_0}$ with $\epsilon_0 > \rho$ a fixed constant, where C depends only on k but independent of ρ. We remark that the estimate in (3.32) would reduce to $C\rho^{1+\delta}$ for $x \in \mathbb{R}^2\backslash\bar{D}_\rho$. Hence, the construction (3.2) is actually a finite realization of the sound-hard lining construction (2.10).

The 3D case could be proved following similar arguments, which we shall sketch in the following. We shall make use of the same notations u_0, u_2, u_{int}, $\tilde{k}$ and k_2 etc.. We have the following series representations of the wave fields,

$$\begin{aligned} u_0(x) =& e^{ikx\cdot d} + u^s(x) \\ =& \sum_{n=0}^{\infty}\sum_{m=-n}^{n} i^n 4\pi \overline{Y_n^m(d)} j_n(k|x|) Y_n^m(\hat{x}) + \sum_{n=0}^{\infty}\sum_{n=-m}^{m} d_n^m h_n^{(1)}(k|x|) Y_n^m(\hat{x}), \\ u_2(x) =& \sum_{n=0}^{\infty}\sum_{m=-n}^{n} a_n^m j_n(\tilde{k}|x|) Y_n^m(\hat{x}) + \sum_{n=0}^{\infty}\sum_{m=-n}^{n} b_n^m h_n^{(1)}(\tilde{k}|x|) Y_n^m(\hat{x}), \\ u_{int}(x) =& \sum_{n=0}^{\infty}\sum_{m=-n}^{n} c_n^m j_n^m(k_2|x|) Y_n^m(\hat{x}). \end{aligned} \tag{3.33}$$

By the transmission conditions, respectively on ∂D_ρ and $\partial D_{\rho/2}$, we have

$$\begin{cases} a_n^m j_n(\tilde{k}\rho) + b_n^m h_n^{(1)}(\tilde{k}\rho) = i^n 4\pi \overline{Y_n^m(d)} j_n(k\rho) + d_n^m h_n^{(1)}(k\rho), \\ \sigma_l \left[\tilde{k} a_n^m j_n'(\tilde{k}\rho) + \tilde{k} b_n^m h_n^{(1)'}(\tilde{k}\rho) \right] = i^n 4\pi k \overline{Y_n^m(d)} j_n'(k\rho) + k d_n^m h_n^{(1)'}(k\rho), \end{cases} \tag{3.34}$$

and

$$\begin{cases} a_n^m j_n(\tilde{k}\rho/2) + b_n^m h_n^{(1)}(\tilde{k}\rho/2) = c_n^m j_n(k_2\rho/2), \\ \sigma_l \left[\tilde{k} a_n^m j_n'(\tilde{k}\rho/2) + \tilde{k} b_n^m h_n^{(1)'}(\tilde{k}\rho/2) \right] = \sigma_a c_n^m k_2 j_n'(k_2\rho/2). \end{cases} \tag{3.35}$$

For this 3D case, we have $A = \sqrt{\sigma_a' q_a'}/\rho^2$, $k_2 = \frac{k}{\rho}\sqrt{\frac{q_a'}{\sigma_a'}}$. Similar to the 2D case (see (3.13), (3.14) and (3.15)), we would solve the linear systems (3.34) and (3.35) and we need to distinguish two cases $j_n(k_2\rho/2) \neq 0$ and $j_n(k_2\rho/2) = 0$. In the following, we only present the more complicated case with $j_n(k_2\rho/2) \neq 0$ and the other case could be handled in a completely similar manner. By solving (3.34) and (3.35), we have

$$d_n^m = -\frac{i^n 4\pi \overline{Y_n^m(d)} j_n'(k\rho) - \frac{1}{C_0} \frac{j_n'(\tilde{k}\rho) + \Upsilon_0 h_n^{(1)'}(\tilde{k}\rho)}{j_n(\tilde{k}\rho) + \Upsilon_0 h_n^{(1)}(\tilde{k}\rho)} i^n 4\pi \overline{Y_n^m(d)} j_n(k\rho)}{h_n^{(1)'}(k\rho) - \frac{1}{C_0} \frac{j_n'(\tilde{k}\rho) + \Upsilon_0 h_n^{(1)'}(\tilde{k}\rho)}{j_n(\tilde{k}\rho) + \Upsilon_0 h_n^{(1)}(\tilde{k}\rho)} h_n^{(1)}(k\rho)}, \tag{3.36}$$

where

$$\Upsilon_0 := -\frac{j_n'(\tilde{k}\rho/2) - C_0 A \frac{j_n'(k_2\rho/2)}{j_n(k_2\rho/2)} j_n(\tilde{k}\rho/2)}{h_n^{(1)'}(\tilde{k}\rho/2) - C_0 A \frac{j_n'(k_2\rho/2)}{j_n(k_2\rho/2)} h_n^{(1)}(\tilde{k}\rho/2)}.$$

By similar asymptotic analyses as those for the 2D case, one can show that as $\rho \to 0^+$,

$$\frac{1}{C_0} \frac{j_n'(\tilde{k}\rho) + \Upsilon_0 h_n^{(1)'}(\tilde{k}\rho)}{j_n(\tilde{k}\rho) + \Upsilon_0 h_n^{(1)}(\tilde{k}\rho)} \to -\frac{1}{C_0} e^{i\pi/2} = -e^{i\pi/2}(\alpha + i\beta)\sqrt{\sigma_l}.$$

Then by (3.36) we have

$$\begin{cases} d_0^0 \sim -\dfrac{-4\pi\overline{Y_0^0(d)}k\rho/3 + 4\pi\overline{Y_0^0(d)}e^{i\pi/2}(\alpha+i\beta)\sqrt{\sigma_l}}{\frac{i}{(k\rho)^2} - e^{i\pi/2}(\alpha+i\beta)\sqrt{\sigma_l}\frac{1}{k\rho}}, \\ d_n^m \sim -\dfrac{i^n 4\pi\overline{Y_n^m(d)}\frac{2^n n!n(k\rho)^{n-1}}{(2n+1)!} + i^n 4\pi\overline{Y_n^m(d)}e^{i\pi/2}(\alpha+i\beta)\sqrt{\sigma_l}\frac{2^n n!(k\rho)^n}{(2n+1)!}}{\frac{i(2n)!(n+1)}{2^n n!(k\rho)^{n+2}} - e^{i\pi/2}(\alpha+i\beta)\sqrt{\sigma_l}\frac{i(2n)!}{2^n n!(k\rho)^{n+1}}}, \end{cases} \tag{3.37}$$

which in turn implies

$$\begin{cases} d_0^0 \sim \mathcal{O}(\rho^3), \\ d_n^m \sim \mathcal{O}(\rho^{2n+1}), \end{cases} \tag{3.38}$$

and

$$\begin{aligned} &\left| d_0^0 - \left[-\frac{4\pi\overline{Y_0^0(d)}j_0'(k\rho)}{h_0^{(1)'}(k\rho)} \right] \right| \le 8\pi k^2 |\alpha+i\beta||Y_0^0(d)|\rho^{3+\delta}, \\ &\left| d_n^m - \left[-\frac{i^n 4\pi\overline{Y_n^m(d)}j_n'(k\rho)}{h_n^{(1)'}(k\rho)} \right] \right| \le \frac{4(2^n n!)^2 4\pi |Y_n^m(d)||\alpha+i\beta|k^{-1-\delta}}{(2n)!(2n+1)!(n+1)}(k\rho)^{2n+3+\delta}. \end{aligned} \tag{3.39}$$

With the above preparations, one can show that the corresponding scattering amplitude corresponding to the cloaking device (3.2) in $\mathbb{R}^3$ satisfies

$$|\mathcal{A}(\hat{x}, d)| \le C\rho^3, \tag{3.40}$$

where C remains uniform as $\rho \to 0^+$. That is, (3.2) gives a near-cloaking device within ρ^3 of the ideal cloaking. Furthermore, by comparing the scattered wave field u^s in (3.33) to that of a 3D sound-hard ball B_ρ (cf. [18]), together with (3.39), one can show that the deviation between them is within $\rho^{3+\delta}$ in $\mathbb{R}^3\backslash\bar{B}_{\epsilon_0}$ for any fixed $\epsilon_0 > \rho$, and within $\rho^{2+\delta}$ in $\mathbb{R}^3\backslash\bar{B}_\rho$. Hence again, we come to the conclusion that the construction (3.2) is a finite realization of the sound-hard lining construction (2.10).

In summary, we have shown in this section that

Theorem 3.1. *Let $D_\rho = B_\rho$ and $\{D_\rho\backslash\bar{D}_{\rho/2}; \sigma_l, q_l\}$ be given by (3.6), and $\{D_{\rho/2}; \sigma_a, q_a\}$ be arbitrary but uniform. Then the construction (3.2) produces a near-cloaking device within ρ^N of ideal cloaking. Furthermore, (3.2) is a finite realization of (2.10) in the sense that the scattered wave fields corresponding to (3.2) and (2.10), respectively, deviate within $\rho^{N+\delta}$ outside the cloaking device.*

As we remarked earlier that Theorem 3.1 equally holds for the general case with general geometry and arbitrary cloaked contents (see [15]). Actually, in the subsequent section, our numerical examples are presented for variable cloaked contents.

4 Some discussion on different cloaking schemes

As we discussed earlier in Section 1, two different cloaking schemes were developed in [12] and [17]. One of the key ingredients is to introduce a special layer between the cloaked region and the cloaking region, which are respectively $D_{1/2}$ and $\Omega\backslash\bar{D}$ in the physical space described in (2.10). They correspond, respectively, $D_{\rho/2}$ and $\Omega\backslash\bar{D}_\rho$ in the virtual space. In [12], the authors introduce a lossy layer occupying $D\backslash\bar{D}_{1/2}$ and they showed that the lossy layer is indispensable to achieve successful near-cloak. In virtual space, the lossy layer in [12] is given as

$$\left\{D_\rho\backslash\bar{D}_{\rho/2}; I, 1+i\beta\right\}, \quad \beta\sim\rho^{-2}. \tag{4.1}$$

If one lets the loss parameter β go to infinity, the limit corresponds to the imposition of a homogeneous Dirichlet boundary condition, which is the one considered in [17]. It is interesting to mention that the improvement of cloaking performance by imposing specific boundary condition on the cloaking interface is also considered in [9]. In this context, imposition of a homogeneous Dirichlet boundary condition amounts to the lining of a layer of sound-soft material in $D_\rho\backslash\bar{D}_{\rho/2}$. In this sense, the lossy layer (4.1) is a finite realization of the sound-soft layer lining. We shall refer the construction in [17] with a sound-soft layer as *SS construction*, and the one in [12] with a finite realization of sound-soft layer as *FSS construction*.

In our cloaking construction (2.10), the inclusion of a sound-hard layer will significantly enhance the cloaking performance, and as specified in the Introduction we call this scheme an SH construction. In order to achieve a finite realization of the sound-hard layer, we utilize the following lossy layer

$$\left\{D_\rho\backslash\bar{D}_{\rho/2}; \sigma_l, a+ib\right\}, \quad \sigma_l\sim\rho^{2+\delta}I, \ \ a\sim 1,\ b\sim 1. \tag{4.2}$$

Clearly, the lossy layer (4.2) is of significant physical and mathematical nature from (4.1), and it could produce significantly improved near-cloaking performances. This losses scheme is called an FSH construction.

5 Numerical examples

In this section, we present some numerical experiments to demonstrate the theoretical results established in the previous sections. There are totally four near-cloak schemes investigated, namely *SS* (sound-soft lining), *FSS* (finite sound-soft lining), *SH* (sound-hard lining) and *FSH* (finite sound-hard lining).

First, all the numerical experiments are conducted in $\mathbb{R}^2$ and we choose D and D_ρ as B_{R_1} and B_ρ, respectively. Some key parameters are set as follows: $R_1 = 2$, $R_2 = 3$ and $R_3 = 4$, thus $R_0 = R_1/2 = 1$. Experimental settings are shown in Figure 1. For the setting with respect to the scattering measurement, a Cartesian PML layer of width 1 is attached to the square $(-5,5)^2$ to truncate the whole space into a finite domain with scattering boundary conditions enforced on the outer boundary. $(-5,5)^2 \setminus \overline{B_{R_3}}$ and $B_{R_3} \setminus \overline{B_{R_2}}$ are homogeneous surrounding media. $B_{R_2} \setminus \overline{B_{R_1}}$ is

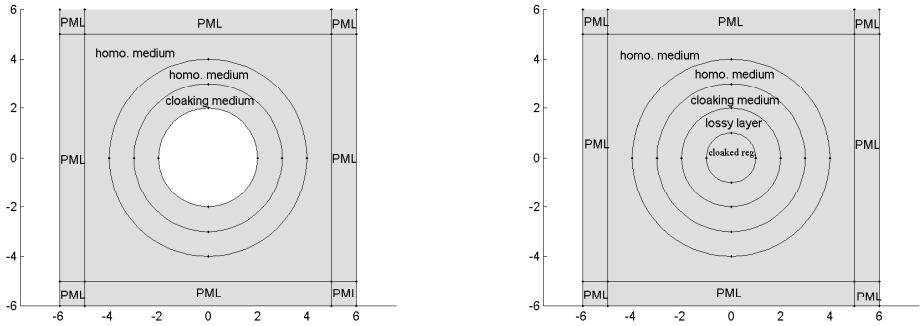

Figure 1: Experimental settings for scattering measurement tests. Left: Tests with *SS* and *SH* lining. Right: Tests with *FSS* and *FSH* lining.

the cloaking medium. $B_{R_1} \setminus \overline{B_{R_0}}$, B_{R_0} are the lossy layer and the cloked region, respectively. The regularization parameter ρ ranges from 0.5 to 10^{-5}. We fix the wave number $k = 2$, and the incident direction $d = (1, 0)^T$.

In addition, for Scheme *FSS*, the lossy parameters are chosen according to [12], i.e., $\sigma_l = I$, $q_l = \rho^2(1 + 2.5\rho^{-2}i)$ in $B_{R_2} \setminus \overline{B_{R_1}}$. For Scheme *FSH*, the lossy parameters are chosen by (3.2), (3.6) and the definition of the map (2.8), namely $\sigma_l = \rho^{2.5} I$, $q_l = \rho^2(3 + 2i)$ in the cloaking medium of the physical space, namely $C = 1$, $\delta = 0.5$, $a = 3$ and $b = 2$.

For Schemes *FSS* and *FSH*, We choose the medium coefficients in the cloaked region to be variable functions $\sigma_a = 1 + 0.3\ x^2y^2$, $q_a = 5 + x$. For Scheme *SH*, the incident wave is shifted to the right by a tenth of the wave length such that the origin is not in the valley nor peak and the incident wave does not vanishes at the origin.

From the transformation map F defined in (2.8), we can determine the cloaking medium coefficients by (3.2) for any $\rho < R_1$. It is emphasized that as ρ tends to zero, the singularity of σ increases very fast. For example, it is observed that σ_{11} grows asymptotically as $1/\rho$ and exhibits a thin layer of large values except some constant background as ρ decreases, which requires many local refinements for better resolution and accounts for the boundary layer in the finite element solutions.

The scattering amplitude, or the far field data, can be computed in the following way (cf. [5]). We can represent the scattered wave in the boundary integral form

$$u^s(x) = \int_{\partial B_{R_3}} u^s(y) \frac{\partial \Phi(x,y)}{\partial \nu(y)} - \Phi(x,y) \frac{\partial u^s(y)}{\partial \nu(y)}\, ds(y), \quad x \in \mathbb{R}^2 \setminus \overline{B_{R_3}}. \tag{5.1}$$

Making use of the asymptotic expansion of the fundamental solution $\Phi(x, y) = iH_0^{(1)}(k|x - y|)/4$, we then have

$$\mathcal{A}(\hat{x}) := \frac{\exp(-i\pi/4)}{\sqrt{8k\pi}} \int_{\partial B_{R_3}} u^s(y) \frac{\partial e^{-ik\hat{x}\cdot y}}{\partial \nu(y)} - e^{-\imath k\hat{x}\cdot y} \frac{\partial u^s(y)}{\partial \nu(y)}\, ds(y), \tag{5.2}$$

where $\hat{x} = x/|x|$ is the observation direction and $\nu(y)$ is the outward unit normal

vector pointing to the infinity. That is, the far field data can be approximated by the numerical quadrature of (5.2) using the Cauchy data of the scattered wave u^s on the boundary of B_3.

Two groups of tests are carried out in the following.

5.1 Near-cloaks of scheme *SS* and scheme *FSS*

It is pointed out that as ρ tends to zero, the medium coefficients exhibit more and more singularity close to ∂B_{R_1}. Thus finite element solutions require more degrees of freedom to resolve the boundary layer close to ∂B_{R_1}. Either the sound-soft boundary condition or the *FSS* lossy layer enforces a strong influence to the local behavior of the transmitted wave close to ∂B_{R_1}, which amounts to introducing a point source in the virtual space. Such *virtual point source* makes the boundary data show a very slow convergence as we decrease ρ. To tackle with the difficulty of the boundary layer amounts to more than two millions of DOF's to achieve the desired relative error tolerance when $\rho = 10^{-5}$. The same observation holds for the other schemes. To avoid the influence of the finite element discretization error, all the following tests are carried out on the finest mesh to show the sharpness of the theoretical error bounds in terms of ρ.

The scattered wave and the transmitted wave are plotted for Schemes *SS* and *FSS*, respectively, for different ρ's in Figures 2.

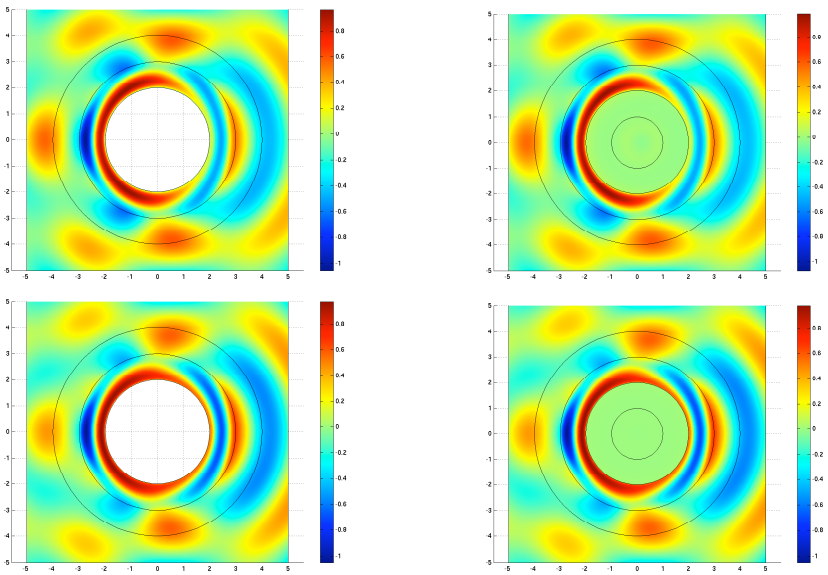

Figure 2: The scattered wave and the transmitted wave (real part) with respect to $\rho = 10^{-1}$ and 10^{-5} from top to bottom, respectively. Left: Scheme *SS*; Right: Scheme *FSS*.

The scattering measurement data are generated according to (5.2) by solving the Helmholtz system on the truncated domain with a PML layer. In the discrete sense,

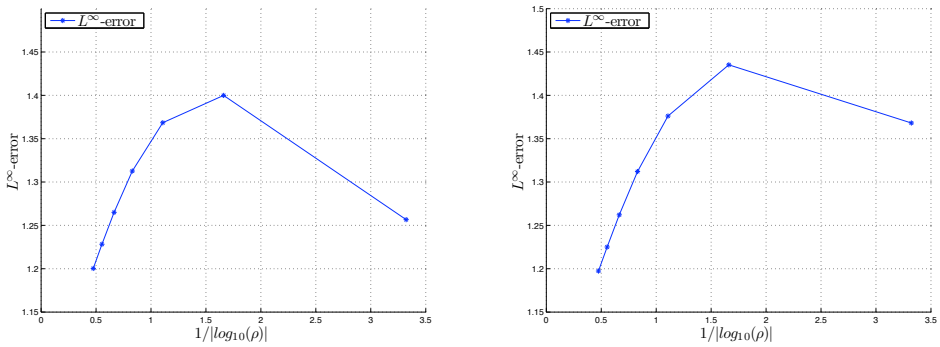

Figure 3: Convergence history of scattering measurement data versus $1/|\log_{10}\rho|$ for Scheme *SS* (Left) and Scheme *FSS* (Right).

all the norms are equivalent. So the discrete maximum norm are used to measure the decay rate of the far field data $\mathcal{A}(\hat{x})$, namely the maximum of the modulus of $\mathcal{A}(\hat{x})$ are taken over 100 equidistant observation direction on $\mathbb{S}^1$. We investigate the convergence rate by testing $\rho = 1/2^j$, $j = 1, 2, \ldots, 7$ for Schemes *SS* and *FSS*. By plotting in Figure 3 the convergence history of the discrete maximum norm of $\mathcal{A}(\hat{x})$ over $\mathbb{S}^1$ with respect to the upper bound $1/|\log_{10}\rho|$, we see clearly that Schemes *SS* and *FSS* schemes indeed achieve near-cloak, but we see that the convergence curve demonstrates linearity asymptotically except the first few outliers to the left of the plots in Figure 3, which verifies the sharpness of the upper bound established in [12]. But the convergence slows down significantly as ρ decreases, which is reflected by the clustering of the blue star points in the curve. More importantly, it can be seen from Figure 3 that the difference between the discrete maximum norms for Schemes *SS* and *FSS* gets smaller as ρ decreases because the *FSS* lossy layer tends effectively to the sound-soft boundary condition for small ρ and thus Scheme *FSS* approaches Scheme *SS* in the limit sense as $\rho \to 0$.

5.2 Near-cloaks of scheme *SH* and scheme *FSH*

Contrary to Schemes *SS* and *FSS*, our new schemes by *SH* and *FSH* lining can achieve significantly better near-cloak performance.

Figure 4 shows the scattered wave and the transmitted wave for Scheme *SH* for different ρ's. Compared with Scheme *SS*, the scattered wave of Scheme *SH* decays significantly as ρ decreases. Moreover, the transmitted wave approaches more and more like a deformed plane incident wave, the interior value of the transmitted wave tends to a constant as $\rho \to 0$.

We plot the scattered wave and the transmitted wave for Scheme *FSH* for different ρ's in Figure 5. We can observe a thin red layer near the outer boundary of the lossy layer, on which both the acoustic potential and the normal flux matches with those from the cloaking medium. Compared with Scheme *FSS*, the scattered wave of Scheme *FSH* decays significantly as ρ decreases. The transmitted wave approaches more and

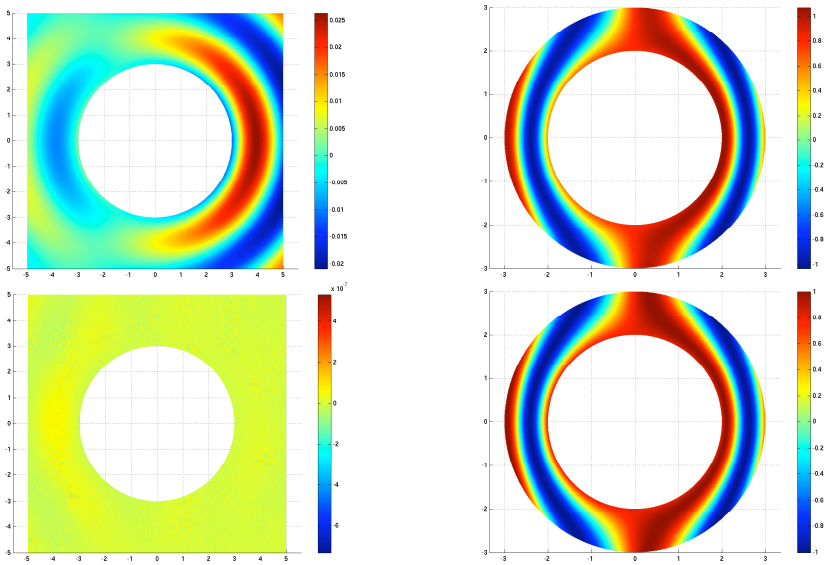

Figure 4: The scattered wave u^s (real part) and the transmitted wave u^t with respect to $\rho = 10^{-1}$ and 10^{-5} from top to bottom, respectively, for *Scheme SH*.

more like a deformed plane incident wave, and the interior acoustic potential of the transmitted wave within the cloaked region vanishes as $\rho \to 0$. In other words, the medium scatterer in the cloaked region is approximately isolated from the exterior world and has negligible affect on the scattering measurement, which means that we achieve significant nearly-invisibility by *SH* and *FSH* constructions.

Finally, we study the convergence history of the discrete maximum norm of $\mathcal{A}(\hat{x})$ with respect to the regularization parameter ρ. From Figure 6, we see clearly second order decay rate of the discrete maximum norm of $\mathcal{A}(\hat{x})$ in terms of ρ for the near-cloak construction Schemes *SH* and *FSH*, compared with the red reference line of second order decay in Figure 6, which confirms the sharpness of our theoretical upper bounds for Schemes *SH* and *FSH*. Similar to their sound-soft counterparts, it can be seen from Figure 6 that the discrete maximum norms for Schemes *SH* and *FSH* have nearly the same values as ρ decreases because the *FSH* lossy layer tends effectively to the sound-hard boundary condition for small ρ and thus Scheme *FSH* approaches Scheme *SH* in the limit sense as $\rho \to 0$. The significantly improved cloaking performance for Schemes *SH* and *FSH* makes it easier for engineers to design practical near-cloak devices in a variety of industrial applications.

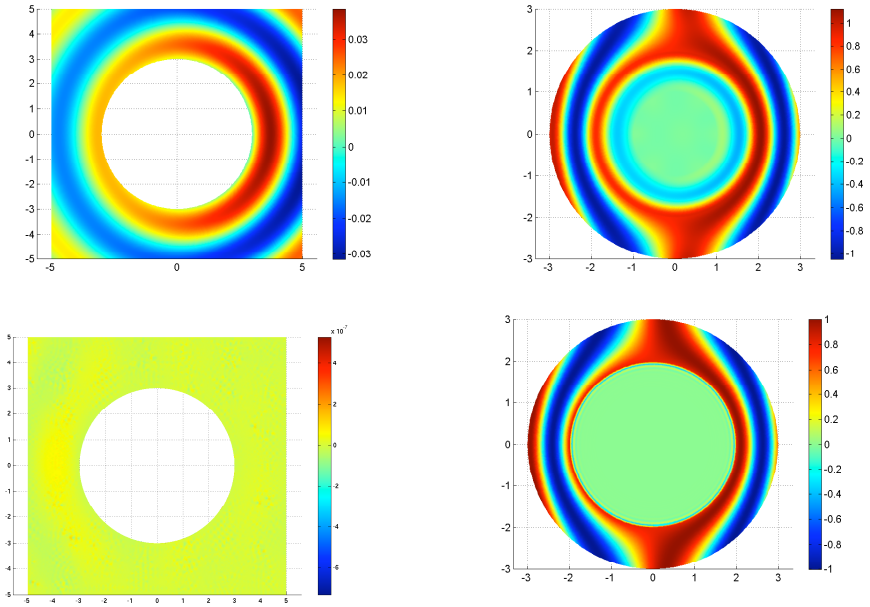

Figure 5: The scattered wave u^s (real part) and the transmitted wave u^t with respect to $\rho = 10^{-1}$ and 10^{-5} from top to bottom, respectively, for *Scheme FSH*.

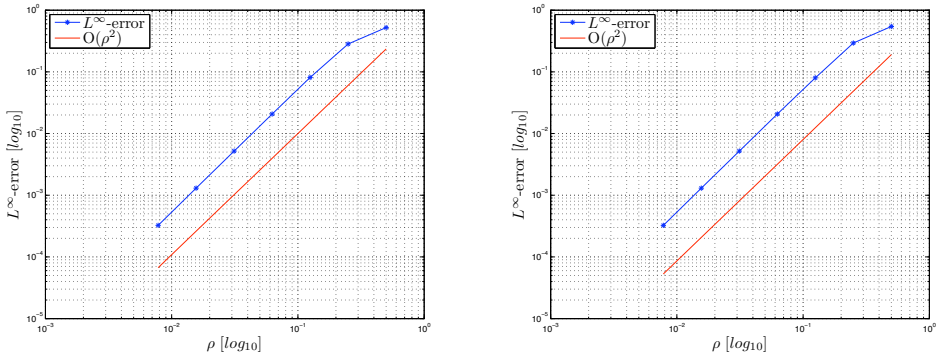

Figure 6: Convergence history of scattering measurement data versus ρ for Scheme *SH* (Left) and Scheme *FSH* (Right).

References

[1] A. Alu and N. Engheta, *Achieving transparency with plasmonic and metamaterial coatings*, Phys. Rev. E, **72** (2005), 016623.

[2] M. Abramowitz and I. A. Stegun, *Handbook of Mathematical Functions*, New York: Dover Publications, 1965.

[3] H. Ammari, H. Kang, H. Lee and M. Lim, Enhancement of near cloaking using generalized polarization tensors vanishing structures. Part I: the conductivity problem, preprint, 2011.

[4] H. Chen and C. T. Chan, *Acoustic cloaking and transformation acoustics*, J. Phys. D: Appl. Phys., **43** (2010), 113001.

[5] D. Colton and R. Kress, *Inverse Acoustic and Electromagnetic Scattering Theory*, 2nd Edition, Springer-Verlag, Berlin, 1998.

[6] A. Greenleaf, Y. Kurylev, M. Lassas and G. Uhlmann, *Isotropic transformation optics: approximate acoustic and quantum cloaking*, New J. Phys., **10** (2008), 115024.

[7] A. Greenleaf, Y. Kurylev, M. Lassas and G. Uhlmann, *Invisibility and inverse prolems*, Bulletin A. M. S., **46** (2009), 55–97.

[8] A. Greenleaf, Y. Kurylev, M. Lassas and G. Uhlmann, *Cloaking devices, electromagnetic wormholes and transformation optics*, SIAM Review, **51** (2009), 3–33.

[9] A. Greenleaf, Y. Kurylev, M. Lassas and G. Uhlmann, *Improvement of cylindrical cloaking with the SHS lining*, Optics Express, **15** (2007), 12717–12734.

[10] A. Greenleaf, M. Lassas and G. Uhlmann, *On nonuniqueness for Calderón's inverse problem*, Math. Res. Lett., **10** (2003), 685.

[11] V. Isakov, *Inverse Problems for Partial Differential Equations*, 2nd Edition, Springer, USA, 2006.

[12] R. Kohn, D. Onofrei, M. Vogelius and M. Weinstein, *Cloaking via change of variables for the Helmholtz equation*, Commu. Pure Appl. Math., **63** (2010), 0973–1016.

[13] R. Kohn, H. Shen, M. Vogelius and M. Weinstein, *Cloaking via change of variables in electrical impedance tomography*, Inverse Problems, **24** (2008), 015016.

[14] P. Lax and R. Phillips, *Scattering Theory*, Academic Press, Inc., San Diego, 1989.

[15] J. Z. Li, H. Y. Liu and H. P. Sun, *Enhanced approximate cloaking for the Helmholtz equation*, forthcoming.

[16] U. Leonhardt, *Optical conformal mapping*, Science, **312** (2006), 1777–1780.

[17] H. Y. Liu, *Virtual reshaping and invisibility in obstacle scattering*, Inverse Problems, **25** (2009), 045006.

[18] H. Y. Liu and J. Zou, *Zeros of Bessel and spherical Bessel functions and their applications for uniqueness in inverse acoustic obstacle scattering*, IMA J. Appl. Math., **72** (2007), 817–831.

[19] W. McLean, *Strongly Elliptic Systems and Boundary Integral Equations*, Cambridge University Press, Cambridge, 2000.

[20] G. W. Milton and N.-A. P. Nicorovici, *On the cloaking effects associated with anomalous localized resonance*, Proc. Roy. Soc. A, **462** (2006), 3027–3095.

[21] A. Nachman, *Reconstruction from boundary measurements*, Ann. Math., **128** (1988), 531–576.

[22] A. Nachman, J. Sylvester, G. Uhlmann, An n-dimensional Borg-Levinson theorem, Comm. Math. Phys., **115** (1988), 595–605.

[23] A. N. Norris, *Acoustic cloaking theory*, Proc. R. Soc. A, **464** (2008), 2411–2434.

[24] J. B. Pendry, D. Schurig and D. R. Smith, *Controlling electromagnetic fields*, Science, **312** (2006), 1780–1782.

[25] Z. Ruan, M. Yan, C. W. Neff and M. Qiu, *Ideal cylyindrical cloak: Perfect but sensitive to tiny perturbations*, Phy. Rev. Lett., **99** (2007), no. 11, 113903.

[26] G. Uhlmann, *Visibility and invisibility*, ICIAM 07–6th International Congress on Industrial and Applied Mathematics, 381408, Eur. Math. Soc., Zürich, 2009.

[27] G. Verchota, *Layer potentials and regularity for the Dirichlet problem for Laplace's equation in Lipschitz domains*, J. Funct. Anal., **59** (1984), 572–611.

[28] M. Yan, W. Yan and M. Qiu, *Invisibility cloaking by coordinate transformation*, Chapter 4 of *Progress in Optics*–Vol. 52, Elsevier, pp. 261–304, 2008.

Research Reports

No.	Authors/Title
11-65	*J. Li, H. Liu and H. Sun* Enhanced approximate cloaking by SH and FSH lining
11-64	*M. Hansen and Ch. Schwab* Analytic regularity and best N-term approximation of high dimensional parametric initial value problems
11-63	*R. Hiptmair, G. Phillips and G. Sinha* Multiple point evaluation on combined tensor product supports
11-62	*J. Li, M. Li and S. Mao* Convergence analysis of an adaptive finite element method for distributed flux reconstruction
11-61	*J. Li, M. Li and S. Mao* A priori error estimates of a finite element method for distributed flux reconstruction
11-60	*H. Heumann and R. Hiptmair* Refined convergence theory for semi-Lagrangian schemes for pure advection
11-59	*V.A. Hoang and Ch. Schwab* N-term Galerkin Wiener chaos approximations of elliptic PDEs with lognormal Gaussian random inputs
11-58	*X. Claeys and R. Hiptmair* Electromagnetic scattering at composite objects: A novel multi-trace boundary integral formulation
11-57	*S. Mishra and L.V. Spinolo* Accurate numerical schemes for approximating intitial-boundary value problems for systems of conservation law
11-56	*P. Grohs* Finite elements of arbitrary order and quasiinterpolation for data in Riemannian manifolds
11-55	*P. Grohs* Bandlimited shearlet-type frames with nice duals
11-54	*A. Kunoth and Ch. Schwab* Analytic regularity and GPC approximation for control problems constrained by linear parametric elliptic and parabolic PDEs
11-53	*Ch. Schwab and S.A. Tokareva* High order approximation of probabilistic shock profiles in hyperbolic conservation laws with uncertain initial data